Far-field Envelope Correlation Coefficient and Near-field Reactive Energy of MIMO Antennas: An FDTD-IDM-CGF Approach

Debdeep Sarkar*[1], Said Mikki[2], Kumar Vaibhav Srivastava[1], Yahia Antar[3]
[1]Department of Electrical Engineering, Indian Institute of Technology, Kanpur, UP, India
[2]Department of Electrical and Computer Engineering, University of New Haven, West Haven, CT, United States
[3]Department of Electrical and Computer Engineering, Royal Military College of Canada, Kingston, ON, Canada
*debdeep1989@gmail.com

***Abstract*—In this paper, a unified procedure to evaluate the far-field envelope correlation coefficient (ECC) and near-field time-domain reactive energy for MIMO antennas is formulated. The proposed approach employs robust finite-difference time-domain (FDTD) modelling of antennas to characterize the local electric / magnetic fields. This is followed by infinitesimal dipole modelling (IDM) of the time-domain radiating antenna currents via equivalence principle. Then, using the recently perceived idea of Cross-correlation Green's functions (CGF) and some time-domain signal processing methods, the wide-band ECC can be calculated directly from the currents for various propagation scenarios. Furthermore, the total energy variation in FDTD volume and analytically calculated radiated power are used to obtain the time-domain reactive energy via an operational energy-subtraction approach. Using the proposed FDTD-CGF-IDM procedure, numerical simulations are performed on single-band and triple-band MIMO antennas based on thin-wire dipoles, which shed light to the connection between inter-element separation of MIMO antennas and wide-band ECC / time-domain reactive energy properties.**

***Index Terms*—Multiple-input multiple-output (MIMO), Cross-correlation Green's function (CGF), Finite-difference time-domain (FDTD), Radiated Power, Reactive energy, Infinitesimal dipole models (IDM).**

I. Introduction

Multiple-input multiple-output (MIMO) antennas have emerged as the backbone of modern-day 4G-Long term evolution (LTE) systems as well as the 5G wireless communication devices that are expecting commercial roll-out by 2020 [1]-[2]. For optimal functioning of MIMO antenna that provides minimum channel capacity loss for stringent bandwidth and SNR levels, it is crucial to reduce the inter-port coupling or $|S_{ij}|$ parameters (i, j being antenna port-indices) in the first level [3]. However the more vital parameter is the far-zone envelope correlation coefficient (ECC or $\rho_{e,ij}$). The ECC embeds the statistical parameters characterizing the propagation scenario (indoor / outdoor, Gaussian / Laplacian etc) in addition to the far-zone radiated fields, implying that ECC is not strictly an electromagnetic artefact [4].

For the ECC ($\rho_{e,ij}$) measurement, recently the idea of Cross-correlation Green's functions (CGF) is introduced in [5] in order to avoid the issues of tedious complex 3D pattern-based post-processing [3] as well as faulty S-parameter based approach [5]. The CGFs enable antenna engineers to obtain ECC information directly from radiating total antenna currents [5]-[6], by constructive the corresponding infinitesimal dipole models (IDM) [7]. This CGF based procedure is further extended for wide-band ECC computation in realistic indoor / outdoor propagation scenario, by integrating with the finite-difference time-domain (FDTD) scheme and modification in the CGFs [8]-[11].

On the other hand, the generalized inter-element mutual coupling (one aspect of which is manifested in port-coupling $|S_{ij}|$) has intrinsic connection with the antenna near-field structure and energy exchange [12]-[17]. Although there are number of unresolved issues yet regarding this antenna reactive energy and near-field coupling mechanisms, most of the discussions on these topics always revolve around frequency domain Q-factors and electrically small antennas [18]. In the studies and critiques of [19]-[21], it is made clear that the near-field analysis of modern-day multi-band / wide-band MIMO systems of non-trivial geometries require a comprehensive time-domain approach, where FDTD is once again the most obvious choice. The first step towards this time-domain reactive energy analysis is carried out in [22]. The main aim of this paper is to unify the different FDTD based computation schemes and thereby demystify some interesting details on the connections of ECC and reactive energy with general antenna interactions in MIMO systems.

II. Brief Description of FDTD-IDM-CGF Methodology

In this section, the FDTD-IDM-CGF procedure for obtaining both the far-field ECC over wide-band and time-domain radiated power $P_{\text{rad}}(t)$, as well as near-field reactive energy $W_{\text{reactive}}(t)$ is described briefly:

1) *FDTD Modeling and Time-marching Simulation:* First the N-port antenna structure of arbitrary shape is modelled in FDTD paradigm, choosing suitable grid size and time-steps that satisfy CFL stability criteria.

2) *IDM construction:* For the various port excitations ($i = 1, 2, \ldots, N$; i = the port index) time-domain infinitesimal dipole models (IDMs) of the antenna radiating currents $\mathbf{J}(\mathbf{r}, t)$ are formulated. This is done utilizing FDTD computed local electric / magnetic fields around the antenna grids, applying surface equivalence principle [23]. For MIMO antenna system, one must compute IDMs for all port-excitations, so that $\rho_{e,ij}$ can be evaluated for any i-th or j-th port combination.
3) *Apply CGF to get ECC:* To obtain frequency variation of ECC or $\rho_{e,ij}$, one needs to apply the concept of CGFs, time-domain signal processing (time-reversal, convolution) and subsequent Fourier transform, on the IDMs for desired i-th and j-th antenna port excitations [8],[11].
4) *Analytically compute time-domain radiated power:* To obtain transient variations of antenna radiated power $P_{\text{rad}}(t)$, the time-domain far-zone electric fields $\mathbf{E}(\mathbf{r}, t)$ from the radiating currents. To obtain this, analytical computation of time-domain magnetic vector potential $\mathbf{A}(\mathbf{r}, t)$ is first performed, followed by the steps discussed in [22], [24].
5) *Compute time-domain reactive energy:* First, the differentiated time-domain total electromagnetic energy in the FDTD computational box dW_{EM}/dt is obtained using the local electric / magnetic fields in time-domain [22]. Then this dW_{EM}/dt, along with the $P_{\text{rad}}(t)$ in the previous step, are applied in an operational energy subtraction approach [22] to finally obtain temporal reactive energy $W_{\text{reactive}}(t)$.

A flow-chart for the entire computational scheme is illustrated in Fig. 1. The detailed equations and their underlying implications are not provided here due to lack of space, and will be discussed in future manuscripts. The next section provides some numerical examples to demonstrate effectiveness of the proposed methodology.

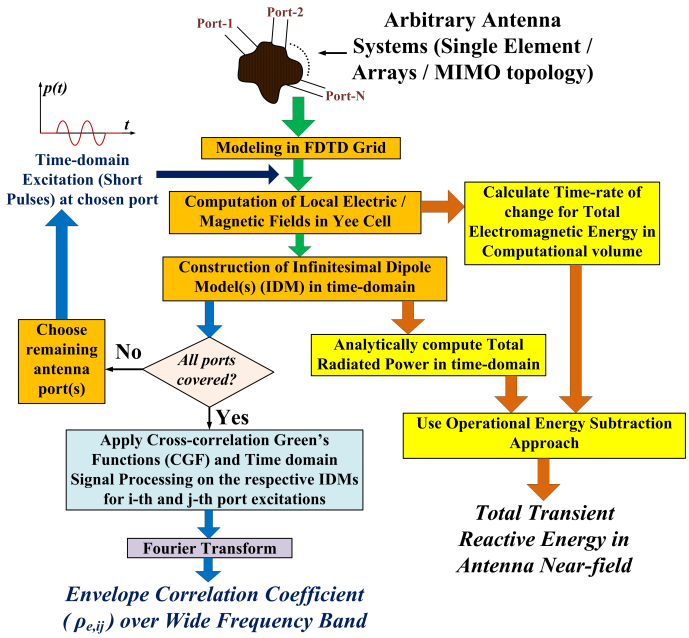

Fig. 1. Flow-chart for the generalized FDTD-IDM-CGF approach for computing both far-field envelope correlation coefficient (ECC) and near-field reactive energy of arbitrary N-port antennas modeled in FDTD paradigm.

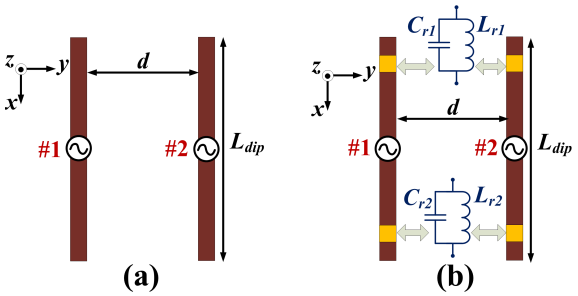

Fig. 2. Schematic diagrams of two-port MIMO systems comprising of two thin-wire x-directed dipoles: (a) Without LC resonator loading (single band) and (b) With two asymmetric LC resonator loading (triple band). The dipole length is $L_{dip} = 37.5$ mm. Three values of inter-element spacing d which will be considered for subsequent simulations are: $d_1 = 7.5$ mm, $d_2 = 12.5$ mm and $d_3 = 17.5$ mm. For the LC resonator loaded dipoles of Fig. 2(b), $x_{off} = 6.3$ mm and $L_{r1} = L_{r2} = 1$ nH, $C_{r1} = 1.5$ pF and $C_{r2} = 2$ pF.

III. Numerical Simulation and Results

Fig. 2 shows the schematics of two MIMO antenna systems where the first one (Fig. 2(a)) comprises of two thin-wire half-wavelength dipoles, each having length L_{dip} and inter-element separation d. The value of L_{dip} is chosen such that the dipole operates in its fundamental mode around 3.68 GHz, which is within one popular sub-6 GHz 5G working band. In the second MIMO system (Fig. 2(b)), the concept of asymmetric LC resonator loading [22] is implemented on the thin wire dipoles to realize triple band functionality. By using suitable values of the lumped loading components (L_{r1}, L_{r2}, C_{r1} and C_{r2}), three working frequencies can be achieved. When one antenna port is excited, the port is terminated with matched load (50Ω). Also for both the MIMO systems, value of d governs the mutual coupling level (S_{21}). The main motive behind the subsequent numerical studies is to observe the effects of variation in d on the various parameters like ECC, mutual coupling as well as temporal profiles of radiated power and reactive energy.

First, the frequency domain metrics: reflection coefficient ($|S_{11}|$), mutual coupling ($|S_{21}|$) and ECC for both the MIMO systems of Fig. 2 are analyzed. Note that the S-parameter analysis here is carried out using our in-house FDTD code, which is benchmarked with commercial full-wave simulator Ansys HFSS. Fig. 3(a) suggests that for $d = d_2 = 12.5$ mm, the single-band MIMO antenna covers the entire sub-6 GHz frequency band of $3.54 - 3.85$ GHz with centre frequency 3.68 GHz. When loaded with LC-resonators as suggested in Fig. 2(b), the triple-band antenna encompasses three narrow frequency bands centered at 3.22 GHz, 3.67 GHz and 4.22 GHz respectively (Fig. 3(b)). It is important to note that variation in d affects the S_{11}-response to some extent, since distance from the parasitic dipole element varies the near-field structure, thereby the input impedance profile for the excited dipole (Fig. 3(a) and Fig. 3(b)). The mutual coupling level

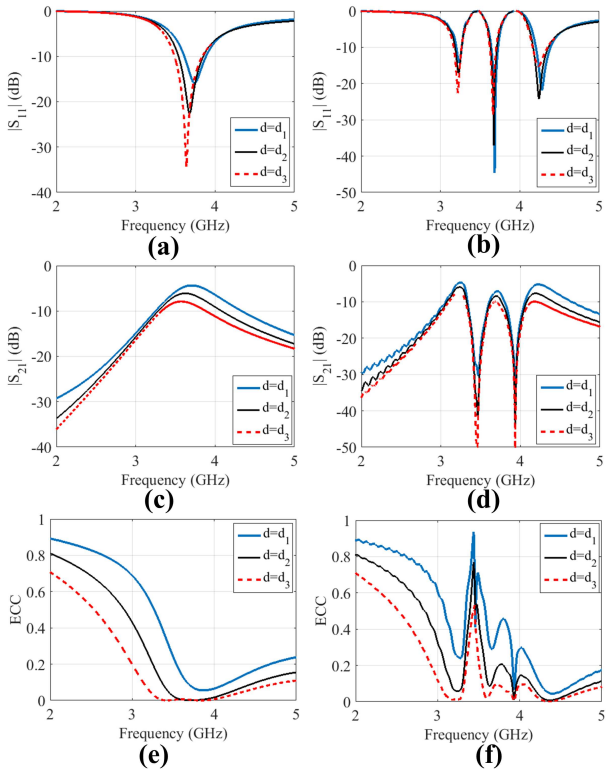

Fig. 3. Simulated $|S_{11}|$ (dB) versus frequency: (a) for Fig. 2(a) and (b) for Fig. 2(b); Simulated $|S_{21}|$ (dB) versus frequency: (c) for Fig. 2(a) and (d) for Fig. 2(b); FDTD-CGF simulated ECC versus frequency: (e) for Fig. 2(a) and (f) for Fig. 2(b). Three values of inter-element spacing d are $d_1 = 7.5$ mm, $d_2 = 12.5$ mm and $d_3 = 17.5$ mm.

is strongly affected by the variation in d for both the single-band and triple-band MIMO antennas (Fig. 3(c)-Fig. 3(d)). It is observed that the maximum mutual coupling ($|S_{21}|_{\max}$) changes by almost 4 dB, when d is varied from 7.5 mm to 12.5 mm (Fig. 3(c)).

Next, the ECC over the entire 2-5 GHz frequency range is evaluated for both the MIMO antennas of Fig. 2 using the FDTD-CGF method in uniform propagation environment [8]. While the previous S-parameter (S_{11} and S_{21}) calculations only require calculation of port-current and voltages, the FDTD-CGF technique requires currents on each infinitesimal dipole element constituting the half-wavelength dipoles [8]. Note that the present-day commercial EM solvers like Ansys HFSS / CST Microwave studio do not yet have such integrated module for wide-band ECC calculation. Fig. 3(e) and Fig. 3(f) suggest that the in-band ECC values get slightly enhanced when the elements come closer to each other, indicating poorer spatial correlation. *Therefore it is evident that both ECC ($\rho_{e,12}$ in this case) and mutual coupling ($|S_{21}|$) performances get detrimental when inter-element separation is reduced.* But the question which now arises is, what impacts are there on the transient radiated power / reactive energy profile, when the mutual separation is changed?

For this purpose, the time-variation of radiated power $P_{\text{rad}}(t)$ and reactive energy $W_{\text{reactive}}(t)$ are examined next for the three values of d for both the single-band and tri-band MIMO antennas of Fig. 2, using the procedure elaborately described in [22]. At this point, two parameters *radiated power enhancement factor* R_{ji} and *reactive energy enhancement factor* W_{ji} are defined as follows:

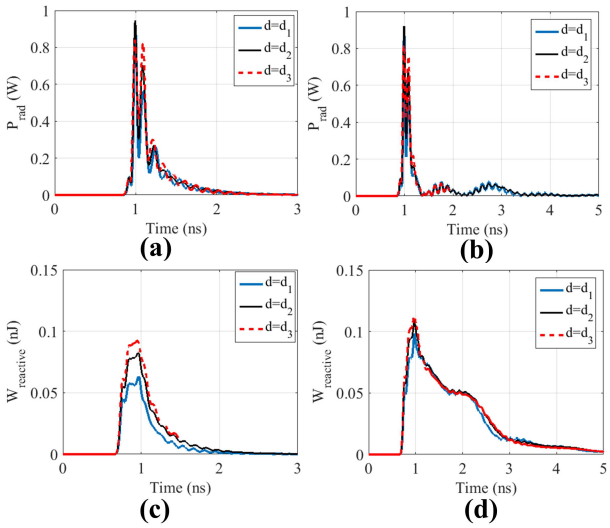

Fig. 4. Temporal variation of radiated power $P_{\text{rad}}(t)$: (a) for Fig. 2(a) and (b) for Fig. 2(b). Temporal variation of reactive energy $W_{\text{reactive}}(t)$: (c) for Fig. 2(a) and (d) for Fig. 2(b).

$$R_{ji} = \frac{\int_0^{T_{\max}} P_{\text{rad},j}(t)dt}{\int_0^{T_{\max}} P_{\text{rad},i}(t)dt} \; ; \; W_{ji} = \frac{\int_0^{T_{\max}} W_{\text{reactive},j}(t)dt}{\int_0^{T_{\max}} W_{\text{reactive},i}(t)dt}. \quad (1)$$

Here i, j refer to the antenna system indices and $T_{\max}$ is the maximum FDTD simulation time, which is chosen sufficiently large so that the transients die out completely. Let us denote the single-band MIMO antennas of Fig. 2(a) for three different d-values (i.e. $d_1 < d_2 < d_3$) as antenna-1, antenna-2 and antenna-3 respectively. The triple-band MIMO antennas of Fig. 2(b) for three different d-values (i.e. $d_1 < d_2 < d_3$) are similarly denoted by antenna-4, antenna-5 and antenna-6 respectively. Some interesting observations can be made from the results in Fig. 4.

The overall radiated energy $\int_0^{T_{\max}} P_{\text{rad}}(t)dt$ slightly increases when d is increased. This underlying reason for this is the reduction in mutual coupling due to increased inter-element separation, which results in increased radiated energy level. This is valid for both the single-band and triple-band MIMO systems ($R_{21} = 1.12$, $R_{31} = 1.19$, $R_{54} = 1.09$ and $R_{64} = 1.13$). Although inclusion of lumped circuit loading introduces a "ringing" nature in the radiated power profile (Fig. 4(b)) as compared to the single-band case (Fig. 4(a)), there is very little change in terms of the overall radiated energy $\int_0^{T_{\max}} P_{\text{rad}}(t)dt$. This is evident from the values $R_{41} = 1.05$, $R_{52} = 1.02$ and $R_{63} = 1.00$. In fact one can see that when placed sufficiently far enough (eg. $d = d_3$), the radiated energy remains almost unchanged, whether the MIMO antenna is single-band or multi-band. Fig. 4(a) and Fig. 4(b) suggest that the inter-element spacing d has observable effects on the $P_{\text{rad}}(t)$ profile. In fact, it is even more clear from Fig. 4(a) that as d increases, the second peak around 1.1 ns is enhanced

quite significantly, while the others get diminished to some extent. However, the number of peaks do remain almost same, irrespective of the d value.

It can be observed from Fig. 4(c) and Fig. 4(d) that the quantity $\int_0^{T_{\max}} W_{\text{reactive}}(t)dt$ significantly increases when lumped circuit loading is introduced in the MIMO system ($W_{41} = 4.78$, $W_{52} = 3.53$ and $W_{63} = 3.09$). However, with increased element spacing values, there is a drop in the enhancement of $\int_0^{T_{\max}} W_{\text{reactive}}(t)dt$ in the triple-band system as compared to the single band one. With increased element spacing the mutual coupling level goes down, which can be seen from the frequency domain results (Fig. 3). However, if one focuses on the single-band MIMO system, there is increase in the quantity $\int_0^{T_{\max}} W_{\text{reactive}}(t)dt$, which is quite apparent from the values of $W_{21} = 1.45$ and $W_{31} = 1.63$ (Fig. 4(c)). *This implies that higher mutual coupling does not always guarantee higher reactive energy levels, in fact the converse is possible*. However, when lumped circuits are used as loading elements, this effect of inter-element spacing on the reactive energy profile is suppressed considerably (this is evident from the values $W_{54} = 1.07$ amd $W_{64} = 1.06$). The reason behind this is the fact that the parallel resonant circuits themselves "store" the significant portion of reactive energy.

IV. Conclusion

A unified FDTD-IDM-CGF approach is presented in this paper (Fig. 1) for computing the wide-band ECC as well as the temporal profiles of radiated power and reactive energy. Starting from the time-domain IDM construction of arbitrary radiating antenna currents, the FDTD-CGF methodology of [8],[11] and energy subtraction approach of [22] are brought into the common framework. Two MIMO antennas realized using single-band and LC-resonator loaded triple-band dipoles are analyzed via the proposed FDTD-IDM-CGF scheme. Some interesting observations, mostly pertaining to the inter-relation between mutual coupling and reactive energy levels of MIMO antennas are obtained. Specifically it is demonstrated that increased inter-element spacing, which causes reduced mutual coupling, may increase the reactive energy level. From the point-of-view of MIMO antenna realization for upcoming 5G base-stations (massive MIMO) or receiver antennas in closely packed handsets, such observations can lead to crucial design insights in future.

References

[1] Q. Li *et al.*, "MIMO techniques in WiMAX and LTE: A feature overview," *IEEE Communication Magazine*, vol. 48, no. 5, pp. 86-92, May 2010.

[2] L. Swindlehurst, E. Ayanoglu, P. Heydari, and F. Capolino, "Millimeter wave massive MIMO: The next wireless revolution?," *IEEE Communication Magazine*, vol. 52, no. 9, pp. 56-62, Sep. 2014.

[3] M. S. Sharawi, "Printed multi-band MIMO antenna systems and their performance metrics," *IEEE Antennas and Propagation Magazine*, vol. 55, no. 5, pp. 218-232, Oct. 2013.

[4] M. A. Jensen and J. W. Wallace, "A Review of Antennas and Propagation for MIMO Wireless Communications," *IEEE Transactions on Antennas and Propagation*, Vol. 52, No. 11, pp. 2810-2824, 2004.

[5] S. M. Mikki and Y. M. M. Antar, "On Cross Correlation in Antenna Arrays With Applications to Spatial Diversity and MIMO Systems," *IEEE Transactions on Antennas and Propagation*, vol. 63, no. 4, pp. 1798-1810, 2015.

[6] S. Clauzier, S. M. Mikki, and Y. M. M. Antar, "A Generalized Methodology for Obtaining Antenna Array Surface Current Distributions With Optimum Cross-Correlation Performance for MIMO and Spatial Diversity Applications," *IEEE Antennas and Wireless Propagation Letters*, vol. 14, pp. 1451-1454, 2015.

[7] S. M. Mikki and A. A. Kishk, "Theory and applications of infinitesimal dipole models for computational electromagnetics," *IEEE Transactions on Antennas and Propagation*, vol. 55, no. 5, pp. 1325-1337, 2007.

[8] D. Sarkar and K. V. Srivastava, "Application of Cross-correlation Green's Function along with FDTD for Fast Computation of Envelope Correlation Coefficient over Wideband for MIMO Antennas," *IEEE Transactions on Antennas and Propagation*, vol. 65, no. 2, pp. 730-740, 2017.

[9] D. Sarkar, S. M. Mikki, K. V. Srivastava and Y. M. M. Antar, "Analytical Approximation of the Time-dependent Antenna Cross-correlation Green's Function," *Proceedings of European Conference on Antennas and Propagation (EuCAP 2018), London, UK*, April 9-13, 2018.

[10] D. Sarkar, S. M. Mikki, K. V. Srivastava and Y. M. M. Antar, "Cross-Correlation Greens Function for Interaction Between Electric and Magnetic Current Sources," *Proceedings of 2018 IEEE International Symposium on Antennas and Propagation and USNC-URSI Radio Science Meeting (APS-URSI 2018), Boston, Massachusetts, USA*, 08-13 July, 2018.

[11] D. Sarkar and K. V. Srivastava, "Modified Cross-correlation Greens Function with FDTD for Characterization of MIMO Antennas in Non-uniform Propagation Environment," *IEEE Transactions on Antennas and Propagation*, vol. 66, no. 7, pp. 3798-3803, 2018.

[12] S. M. Mikki and Y. M. M. Antar, *New Foundations for Applied Electromagnetics: The Spatial Structure of Fields*, Artech House, London, 2016.

[13] S. M. Mikki and Y. M. M. Antar, "A Theory of Antenna Electromagnetic Near Field-Part I," *IEEE Transactions on Antennas and Propagation*, vol. 59, no. 12, pp. 4691-4705, 2011.

[14] S. M. Mikki and Y. M. M. Antar, "A Theory of Antenna Electromagnetic Near Field-Part II," *IEEE Transactions on Antennas and Propagation*, vol. 59, no. 12, pp. 4706-4724, 2011.

[15] S. M. Mikki and Y. M. M. Antar, "Near-Field Analysis of Electromagnetic Interactions in Antenna Arrays Through Equivalent Dipole Models," *IEEE Transactions on Antennas and Propagation*, vol. 60, no. 3, pp. 1381-1388, 2012.

[16] S. M. Mikki and Y. M. M. Antar, "Physical and Computational Aspects of Antenna Near Fields: The Scalar Theory," *Progress In Electromagnetics Research B*, vol. 63, pp. 67-78, 2015.

[17] S. M. Mikki and Y. M. M. Antar, "A New Technique for the Analysis of Energy Coupling and Exchange in General Antenna Systems," *IEEE Transactions on Antennas and Propagation*, vol. 63, no. 12, pp. 5536-5547, 2015.

[18] K. Schab, L. Jelinek, M. Capek, C. Ehrenborg, D. Tayli, G. A. E. Vandenbosch, and M. Gustafsson, "Energy Stored by Radiating Systems," *IEEE Access*, Vol. 6, pp. 10553-10568, 2018.

[19] A. M. Alzahed, S. M. Mikki, and Y. M. M. Antar, "Stored Energy in General Antenna System: A New Approach," *Proceedings of European Conference on Antennas and Propagation (EuCAP)*, pp. 1-4, 2016.

[20] S. M. Mikki, A. M. Alzahed, and Y. M. M. Antar, "Radiation energy of antenna fields: critique and a solution through recoverable energy," *International Union of Radio Science General Assembly & Scientific (URSI) Symposium*, Montreal, August 2017.

[21] D. Sarkar, S. M. Mikki, A. M. Alzahed, K. V. Srivastava, Y. M. M. Antar, "New Considerations on Electromagnetic Energy in Antenna Near-Field by Time-Domain Approach," *Proceedings of IEEE Applied Electromagnetics Conference (IEEE AEMC 2017), Aurangabad, India*, 19-23 December 2017.

[22] D. Sarkar, S. M. Mikki, K. V. Srivastava and Y. M. M. Antar, "Dynamics of Antenna Reactive Energy Using Time Domain IDM Method," *IEEE Transactions on Antennas and Propagation*, 2018 (In Press).

[23] C. A. Balanis, *Antenna Theory: Analysis and Design*, 3rd edition, Wiley Inter-science.

[24] J. D. Jackson, *Classical Electrodynamics*, 3rd edition, New York, NY: Wiley.